PHYSICAL REVIEW B **81**, 241307(R) (2010)

Electric field tuned crossover from classical to weakly localized quantum transport in electron doped $SrTiO_3$

J. H. Ngai,[1] Y. Segal,[1] D. Su,[2] Y. Zhu,[2] F. J. Walker,[1] S. Ismail-Beigi,[1,3] K. Le Hur,[1,3] and C. H. Ahn[1,3]
[1]*Department of Applied Physics, Center for Research on Interface Structures and Phenomena, Yale University, 15 Prospect Street, New Haven, Connecticut 06520-8284, USA*
[2]*Center for Functional Nanomaterials, Brookhaven National Laboratory, Upton, New York 11973, USA*
[3]*Department of Physics, Yale University, 217 Prospect Street, New Haven, Connecticut 06511-8499, USA*
(Received 23 April 2010; published 21 June 2010)

Electron gases created by modulating the charge density near interfaces and surfaces of insulating $SrTiO_3$ offer a wide range of tunable behavior. Here, we utilize the nonlinear dielectric response of $SrTiO_3$ to electrostatically manipulate the spatial confinement of an electron gas relative to an interface, where scattering is enhanced. Magnetotransport measurements reveal that the electron gas can be tuned from weakly localized to classical transport regimes. This crossover in transport demonstrates that elastic scattering can be electrostatically controlled, providing another degree of tunability for electron gases in $SrTiO_3$.

DOI: 10.1103/PhysRevB.81.241307 PACS number(s): 71.10.Ca, 68.47.Gh, 75.47.−m

I. INTRODUCTION

Transition-metal oxides exhibit extraordinary functionality that can be tuned through charge-carrier doping.[1] A well-known example of such a compound is $SrTiO_3$ (STO), which transitions from insulating to semiconducting behavior as electrons are progressively doped into the lattice through oxygen vacancies or chemical substitution.[2] Recent advances have enabled quasi-two-dimensional electron gases (Q2DEGs) to be created by modulating the carrier density near interfaces and surfaces of insulating STO.[3–15] In particular, much interest has focused on the Q2DEG found at the $LaAlO_3$ (LAO)/STO interface,[3–11] where indications of magnetism and superconductivity have been observed.[7,8] Q2DEG's in STO can also be created through Ar irradiation,[12–15] which have been found to exhibit photoluminescent behavior.[13] Q2DEG's can potentially be utilized in future electronic devices, provided methods to control the rich phenomena they exhibit are developed and understood.

In this regard, the dielectric properties of STO can be used to tune the behavior of Q2DEG's. For example, by applying an electrostatic field, the insulating STO can serve as a capacitor to gate dope the Q2DEG.[4,8] An electrostatic field is also expected to change the spatial thickness of the Q2DEG by modifying the potential that confines the carriers.[10] The nonlinear dielectric constant $\epsilon(E)$ of STO, which decreases rapidly with electric field,[16] could amplify this change in confinement. According to Poisson's equation, small (large) ϵ generally gives rise to a deep (shallow) confinement potential. Thus, a *large* change in confinement could, in principle, be induced by modulating $\epsilon(E)$ with a *small* electrostatic field. Of particular interest is the intriguing possibility of manipulating the spatial proximity of carriers with respect to an interface, where scattering is enhanced. Such an effect could enable scattering to be electrostatically controlled, providing another degree of tunability for Q2DEG's in STO.

To explore this possibility, we present low-temperature magnetotransport measurements of Ar-irradiated STO under an applied electrostatic field. Ar irradiation creates a thin layer of oxygen vacancies near the irradiated surface, resulting in a Q2DEG. We find that the mobility μ, or carrier relaxation time $\tau \propto \mu$, can be modulated by a factor of ~ 50 through a modest applied electric field ($\pm 4 \times 10^5$ V/m). Magnetoresistance (MR) measurements, which provide insight on the observed modulation of μ, show that a crossover from classical to weakly localized quantum transport is induced as carriers are confined close to the interface. The nonlinear $\epsilon(E)$ enhances the confinement by a factor of 2, as shown through numerical solutions to the Poisson and Schrödinger equations. These results elucidate the combined effects of an electrostatic field and the nonlinear $\epsilon(E)$ on the confinement of and scattering within Q2DEG's.

II. EXPERIMENTAL PROCEDURE

A schematic of our Ar-irradiated devices is shown in Fig. 1(a). The 80×40 μm^2 Hall bar is defined using standard photolithography on a 0.5-mm-thick substrate. The device becomes conducting after irradiation with 1 keV Ar ions at a rate of $\sim 3.7 \times 10^{12}$ cm^{-2} s^{-1} for 90 min. Figure 1(b) shows a low-angle annular dark field image (LAADF) of our device, obtained through cross-sectional scanning transmission electron microscopy (STEM). An abrupt interface of ~ 1 unit cell roughness separates a ~ 5-nm-thick, amorphous layer (circle), from a ~ 5-nm-thick, crystalline layer of oxygen-deficient STO (triangle).[17] Although, the majority of dopant vacancies are limited to this ~ 5 nm oxygen-deficient region, we will show that the carriers can be electrostatically pulled ~ 270 nm into the undoped crystal (square). The sheet resistance of the amorphous layer exceeds $\sim 10^9$ Ω at $T = 2$ K, thus the conduction occurs in the crystalline regions.[18] Ohmic contacts are formed by wire bonding Al wires directly to the STO, which penetrates the amorphous layer. The gate contact is made by depositing Au on the backside of the device. At 2 K, V_G is first ramped between ± 210 V to reduce charge trapping in the STO and minimize hysteresis in the gating. Gate leakage currents are < 1 nA for all V_G. Representative data from one of the devices are shown in the figures below.

 ©2010 The American Physical Society

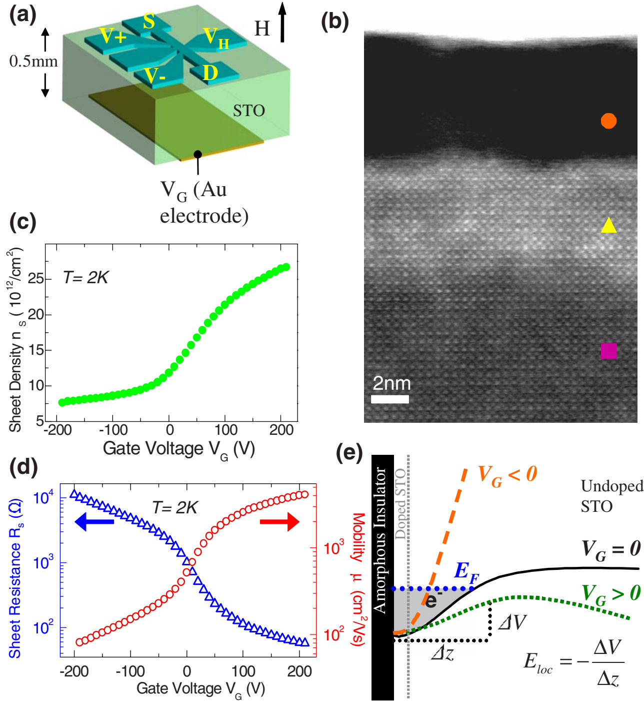

FIG. 1. (Color online) Characterization of Ar-irradiated STO devices. (a) Schematic of device. (b) LAADF STEM image of device with amorphous (circle) and crystalline-doped (triangle) and undoped (square) regions indicated. (c) Sheet carrier density versus V_G. (d) Sheet resistance (mobility) versus V_G shown as triangles (circles). (e) Illustration of potential confining carriers (e^-, gray shaded) with $V_G>0$ ($V_G<0$) case shown as dotted (dashed) curve. For $V_G>0(V_G<0)$ E_{loc} is small (large) thus $\epsilon(E)$ is large (small). The difference in $\epsilon(E)$ between the $V_G>0$ and $V_G<0$ cases gives rise to a large change in confinement and scattering.

III. RESULTS AND DISCUSSION

Hall and sheet resistance (R_s) measurements reveal the modulation in μ. Figure 1(d) indicates that R_s (triangles) can be modulated by over two orders of magnitude between $-190 \leq V_G \leq 210$ V. For positive (negative) V_G, R_s decreases (increases), consistent with the addition (removal) of n-type carriers to (from) the channel of the device according to the relation $R_s=(n_s e\mu)^{-1}$, where e is the electron charge. Hall measurements at each V_G directly determined Δn_s, which is related to the Hall coefficient through $\Delta R_H=(-\Delta n_s e)^{-1}$. We find that n_s can be tuned by a factor of ~ 3 from ~ 8 to $\sim 27\times 10^{12}$ cm^{-2} for $-190 \leq V_G \leq 210$ V as shown in Fig. 1(c). This rather modest Δn_s cannot account for ΔR_s, thus V_G also modulates μ, as shown in Fig. 1(d) (circles).[19] For the representative device shown, μ could be modulated by a factor of ~ 50 from ~ 80 to ~ 4100 cm^2/V s.

MR measurements provide insight on the modulation of μ. The MR, defined as $\Delta R_s(H)/R_s(0)$, where $\Delta R_s(H)=R_s(H)-R_s(0)$, is shown in Fig. 2 as a function of magnetic field $B=\mu_0 H$ applied out of the plane of the device for various V_G. Positive MR is observed in the high-μ regime associated with $V_G>0$. In contrast, negative MR is observed in the low-μ regime associated with $V_G \ll 0$.

Classical transport characterized by a scaling of the MR is observed in the high-μ data shown in Fig. 3(a). We show this scaling by plotting the MR data against $\mu \times B$ in Fig. 3(b). The data at each V_G collapse virtually onto a common curve indicating that Kohler's rule is obeyed, i.e., the MR is a function of $B\tau$, $\Delta R_s(B)/R_s(0)=F(B\tau)$.[20] At weak fields, the MR exhibits classical B^2 dependence, described by $F=A(\mu B)^2=A(\omega_c\tau)^2$, where ω_c is the cyclotron frequency and $A\sim 0.37$, as determined by the fit in Fig. 3(b) (gray dotted).[21]

The scaling of the MR with V_G can be correlated with a change in carrier confinement. In the high-μ regime, the confinement can be estimated by examining the MR for magnetic fields applied parallel to the current between source and

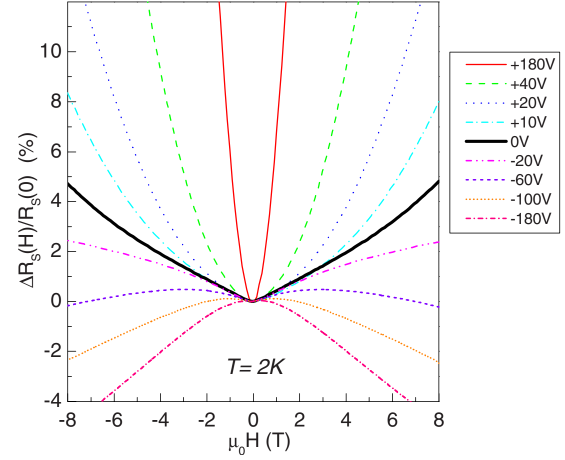

FIG. 2. (Color online) Electrostatic modulation of the MR of Ar-irradiated $SrTiO_3$ at $T=2$ K. A crossover from classical to weakly localized quantum transport is observed going from high- to low-μ regimes.

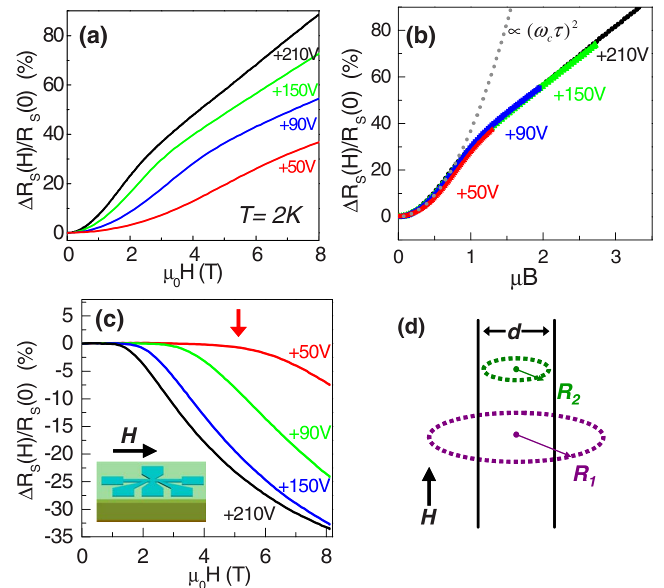

FIG. 3. (Color online) High-μ regime MR of Ar-irradiated $SrTiO_3$ at $T=2$ K. (a) Evolution of MR with V_G. (b) Kohler plot of MR with weak field $\propto(\omega_c\tau)^2$ fit (gray dotted) indicating classical behavior. (c) In-plane MR. Red arrow indicates onset of negative MR for $V_G=+50$ V indicating reduction in boundary scattering. (d) Cross-sectional illustration of a thin conducting plate of thickness d. Orbital radius $R_1>(d/2)$ $[R_2<(d/2)]$.

drain (I_{DS}) in the plane of the device, as shown in the inset of Fig. 3(c). In this geometry, the Lorentz force associated with B does not scatter the component of carrier momentum parallel to I_{DS}. We observe negative MR that develops beyond a threshold field B^*, which varies with V_G. For example, $B^* \sim 5.5$ T for the $V_G = +50$ V curve (red), as shown by the red arrow in Fig. 3(c). In high-μ, nonmagnetic systems, negative in-plane MR can arise from a reduction in the scattering of charge carriers at the sample boundaries.[22] The dependence of B^* on V_G is understood if we consider the channel as a plate of thickness d, as shown in Fig. 3(d). The charge carriers follow helical paths of radii $R \propto B^{-1}$ induced by the Lorentz force of the in-plane field. A reduction in boundary scattering occurs for carriers of orbital radii $R \leq d/2$. Thus, d in the high-μ regime can be estimated by relating B^* to the classical cyclotron radius,[23]

$$d \sim 2\left[\frac{3\pi^2 n_s \hbar^3}{2e^3 (B^*)^3}\right]^{1/4}. \tag{1}$$

From Eq. (1) we find that d increases from ~ 90 nm at $V_G = +50$ V to ~ 270 nm at $V_G = +210$ V. Our interpretation of B^* rests on the premise of quasiballistic transport, i.e., $d \sim l$, the mean-free path. We calculate l and find $d \sim 2l (\sim 4l)$ for $V_G = +50$ V(+210 V), which confirms our analysis is self-consistent.

This change in confinement induced by V_G can be understood if we consider the carrier potential as a function of depth z near the interface, illustrated in Fig. 1(e). The carriers occupy states in the conduction band of STO, which bends at the interface due to the built-in potential associated with oxygen vacancies (black solid curve). V_G directly modifies the bending of the conduction band due to the continuity of the band between the Q2DEG and the insulating crystal. For $V_G > 0 (V_G < 0)$, the local electric field E_{loc} arising from the built-in potential is weakened (augmented) near the interface, resulting in decreased (increased) confinement, as illustrated by the dotted (dashed) curve. The nonlinear $\epsilon(E)$ amplifies the effect of V_G in modulating E_{loc}. For $V_G > 0 (V_G < 0)$, E_{loc} near the interface is small (large), thus ϵ is large (small). Large (small) ϵ further decreases (increases) the confinement. Thus, for $V_G > 0 (V_G < 0)$, carriers are pulled away from (confined near) ionized dopants and the interface, giving rise to significant changes in scattering.

The effects of increased scattering due to enhanced confinement are seen in the MR for $V_G < 0$. The Kohler plot of Fig. 4(a) shows the emergence of negative MR and deviation from Kohler's rule. The latter, denoting a departure from classical behavior, is tied to the origin of the former, which can be understood in terms of the elastic τ_e and inelastic τ_i relaxation times that comprise τ. As confinement increases, enhanced elastic scattering at the interface dramatically decreases τ_e relative to τ_i, the latter being largely temperature dependent. In the limit where $\tau_e \ll \tau_i$, carriers can be coherently backscattered. Weak localization occurs as time-reversed pairs of backscattered carriers constructively interfere.[25] This constructive interference is suppressed by $\mu_0 H$, which introduces phase shifts of opposite sign to time-reversed pairs, resulting in negative MR. We fit the $V_G = -190$ V data to two-dimensional weak localization formalism in Fig. 4(b), specifically Eq. (5) in Bishop *et al.*[24] The parameter $l_e(l_i)$ is the elastic (inelastic) scattering length defined as $l_e = v_F \tau_e (l_i = v_F \tau_i)$, where v_F is the Fermi velocity. The excellent fit indicates that the confinement, or thickness of the Q2DEG, is approaching the phase coherence length $L_\phi = \sqrt{0.5 l_e l_i} \sim 10$ nm.

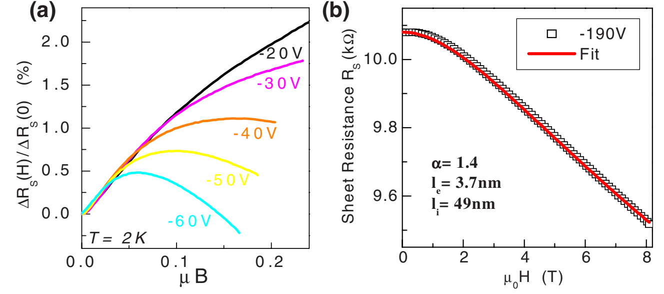

FIG. 4. (Color online) Low-μ regime MR of Ar-irradiated $SrTiO_3$ at $T = 2$ K. (a) Kohler plot of MR showing violation of Kohler's rule. (b) Sheet resistance for $V_G = -190$ V (squares) with fit (solid curve) using Eq. (5) of Bishop *et al.* (Ref. 24) indicating 2D weak localization. Magnitude α, elastic l_e, and inelastic l_i scattering lengths are indicated.

To gain insight on how the nonlinear $\epsilon(E)$ enhances the confinement for $V_G < 0$, we self-consistently solve the Poisson and Schrödinger equations for the carrier density $\rho(z)$. We model our device as a 300-nm-thick slab where $z = 0(-300$ nm) represents the crystalline/amorphous interface (backside) of the device. $\rho(z)$ is obtained from $\rho(z) = \frac{m^*}{\pi\hbar^2} \Sigma_i (E_F - E_i) |\psi_i(z)|^2$, where the subband energies E_i and $\psi_i(z)$ are found by numerically diagonalizing the Schrödinger equation. E_F is determined by filling occupied subbands i until n_s is reached. In our calculations, Δn_s arising from the capacitive effect of STO is taken into account by using n_s values obtained by Hall measurements. An effective mass of $m^* = 4m_e$ is used, where m_e is the bare electron mass.[26] The carrier potential V is found by iteratively solving the Poisson $\nabla^2 V = -\rho_f(z)/\epsilon(E)$ and Schrödinger equations. $\rho_f(z)$ is comprised of $\rho(z)$ as well as oxygen vacancies represented by a positive dopant profile $\rho_{dop}(z) \propto \exp(\frac{z}{\kappa})$ for $z < 0$, as shown in Fig. 5(b) (bold). κ is set to 5 nm, as determined from the oxygen-deficient region shown in Fig. 1(b) (triangle). To model the effect of V_G on V, a sheet charge density N_G is placed at the backside of the slab. N_G is related to V_G through $N_G = \int_{V_G}^{0} C(V) dV$, where $C(V)$ is the measured capacitance of our device. We find that for $V_G = -210$ V, $N_G \sim 2.2 \times 10^{13}$ cm^{-2}. In order to maintain charge neutrality, $\rho_{dop}(z)$ is enhanced for $V_G = -210$ V, as shown in Fig. 5(b) (dashed). This enhancement of $\rho_{dop}(z)$ can be associated with charge trapping sites that become ionized with V_G. Finally, the nonlinear dielectric response is captured via $\epsilon[E(z)] = 1 + (\epsilon_0^{-1}) \partial P / \partial E$, where P is related to $E(z)$ through the Landau-Ginzburg-Devonshire free energy.[16]

$\rho(z)$ is shown in Fig. 5(a) for the $V_G = 0$ (solid) and -210 V (bold) cases calculated with the nonlinear $\epsilon(E)$. To elucidate the effect of $\epsilon(E)$ on confinement, Fig. 5(a) shows $\rho(z)$ for $V_G = 0$ (dotted) and -210 V (dashed) calculated using a constant $\epsilon = 24\,000\epsilon_0$. In comparing $\rho(z)$'s between the constant ϵ and $\epsilon(E)$ cases, an enhancement in confinement by

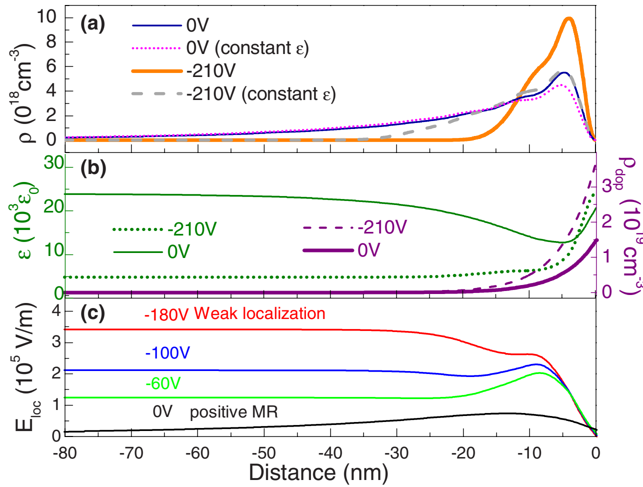

FIG. 5. (Color online) Calculated carrier density $\rho(z)$ near the amorphous/crystalline interface ($z=0$) for $V_G \leq 0$. (a) $\rho(z)$ for $V_G=0$ (solid), -210 V (bold) using nonlinear $\epsilon(E)$. $\rho(z)$ for $V_G=0$ (dotted) and -210 V (dashed) with $\epsilon=24\,000\epsilon_0$. (b) $\epsilon(z)$ for $V_G=0$ (solid), -210 V (dotted), as well as dopant density $\rho_{dop}(z)$ for $V_G=0$ (bold), -210 V (dashed). (c) Local electric field E_{loc} for various V_G.

a factor ~ 2 is clearly seen for $V_G=-210$ V. Thus we conclude that the nonlinear dielectric response of STO is essential to achieve 2D weak localization, i.e., confinement that approaches L_ϕ. The spatial dependence of $\epsilon(E)$ for the $V_G=0$ (solid) and $V_G=-210$ V (dotted) cases are shown in Fig. 5(b). The variation in E_{loc} with V_G, which induces the change in $\epsilon(E)$, is shown in Fig. 5(c). The decrease in E_{loc} indicates the crossover from weakly localized to positive MR in our devices is not consistent with a Rashba effect.[27]

We have demonstrated that the effect of a relatively modest field of $\pm 4 \times 10^5$ V/m can be amplified by a nonlinear dielectric response to sweep carriers between low-μ interface and high-μ bulk regions. Q2DEG's could thus be utilized in so-called velocity modulated transistors, where changes in μ determine channel conductance.[28] The change in scattering enhanced by $\epsilon(E)$ likely contributes to the electrostatic modulation of superconductivity at the LAO/STO interface, as suggested by recent experiments.[10]

IV. SUMMARY

In summary, we have electrostatically controlled elastic scattering in electron doped STO to induce a crossover from classical to weakly localized quantum transport. This effect, made possible by the nonlinear dielectric response of STO, provides another degree of tunability for electron gases in STO.

ACKNOWLEDGMENTS

We thank J.-M. Triscone and S. Gariglio for discussions and K. Kisslinger for TEM sample preparation. J.H.N acknowledges funding from NSERC. This work was supported by the NSF under Contract No. MRSEC DMR-0520495, the DOE under Contract No. DE-AC02-98CH10886, and the FENA center.

[1] C. H. Ahn *et al.*, Nature (London) **424**, 1015 (2003).
[2] O. N. Tufte and P. W. Chapman, Phys. Rev. **155**, 796 (1967).
[3] A. Ohtomo and H. Y. Hwang, Nature (London) **427**, 423 (2004).
[4] S. Thiel *et al.*, Science **313**, 1942 (2006).
[5] G. Herranz *et al.*, Phys. Rev. Lett. **98**, 216803 (2007).
[6] W. Siemons, G. Koster, H. Yamamoto, W. A. Harrison, G. Lucovsky, T. H. Geballe, D. H. A. Blank, and M. R. Beasley, Phys. Rev. Lett. **98**, 196802 (2007).
[7] A. Brinkman *et al.*, Nature Mater. **6**, 493 (2007).
[8] A. D. Caviglia *et al.*, Nature (London) **456**, 624 (2008).
[9] J. W. Reiner *et al.*, Science **323**, 1018 (2009).
[10] C. Bell, S. Harashima, Y. Kozuka, M. Kim, B. G. Kim, Y. Hikita, and H. Y. Hwang, Phys. Rev. Lett. **103**, 226802 (2009).
[11] Y. Segal, J. H. Ngai, J. W. Reiner, F. J. Walker, and C. H. Ahn, Phys. Rev. B **80**, 241107(R) (2009).
[12] D. W. Reagor and V. Y. Butko, Nature Mater. **4**, 593 (2005).
[13] D. Kan *et al.*, Nature Mater. **4**, 816 (2005).
[14] M. Schultz and L. Klein, Appl. Phys. Lett. **91**, 151104 (2007).
[15] V. Y. Butko *et al.*, Nanotechnology **19**, 305401 (2008).
[16] H.-M. Christen, J. Mannhart, E. J. Williams, and C. Gerber, Phys. Rev. B **49**, 12095 (1994).
[17] D. A. Muller *et al.*, Nature (London) **430**, 657 (2004).
[18] Ar-irradiated thin STO grown on LSAT shows insulating behavior. Y. Segal (unpublished).
[19] We note that ionic conduction of oxygen at $T=2$ K is highly unlikely since ionic conductivity follows $\sigma_{ion} \propto \exp(\frac{-E_a}{k_B T})$, where $E_a \sim 0.5-1$ eV (Ref. 29).
[20] R. G. Chambers, Proc. R. Soc. London, Ser. A **238**, 344 (1956).
[21] E. H. Putley, *The Hall Effect and Semi-Conductor Physics* (Dover, New York, 1968), Chap. 3.
[22] D. K. C. MacDonald, Nature (London) **163**, 637 (1949); M. C. Steele, Phys. Rev. **97**, 1720 (1955); A. N. Friedman and S. H. Koenig, IBM J. Res. Dev. **4**, 158 (1960).
[23] We begin with $d=2R=2\frac{m^* v_F}{e(\mu_0 B^*)}$, the classical cyclotron orbital radius R at B^* with three-dimensional Fermi velocity $v_F = \frac{\hbar}{m^*}(3\pi^2 n)^{1/3}$. The carrier concentration n, is approximated to be $n=n_s/d$, which then results in Eq. (1).
[24] D. J. Bishop, R. C. Dynes, and D. C. Tsui, Phys. Rev. B **26**, 773 (1982). We fit using only the third term on the right-hand side of Eq. (5).
[25] P. A. Lee and T. V. Ramakrishnan, Rev. Mod. Phys. **57**, 287 (1985).
[26] L. F. Mattheiss, Phys. Rev. B **6**, 4718 (1972).
[27] T. Koga, J. Nitta, T. Akazaki, and H. Takayanagi, Phys. Rev. Lett. **89**, 046801 (2002).
[28] H. Sakaki, Jpn. J. Appl. Phys., Part 2 **21**, L381 (1982).
[29] F. Cordero, Phys. Rev. B **76**, 172106 (2007).